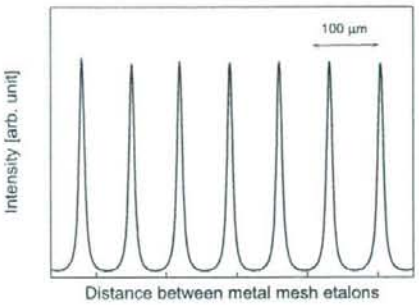

Fig. 7 An example of wavelength and linewidth measurement by scanning Fabry-Perot etalon consisting if two metal mesh plate.

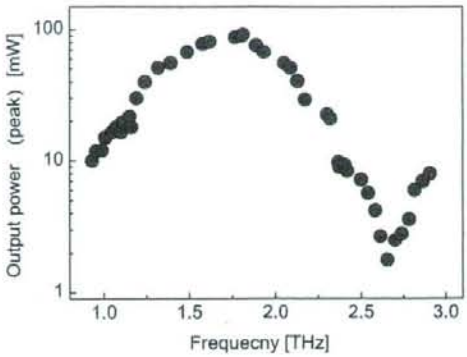

Fig. 8 Tunability of an is-TPG.

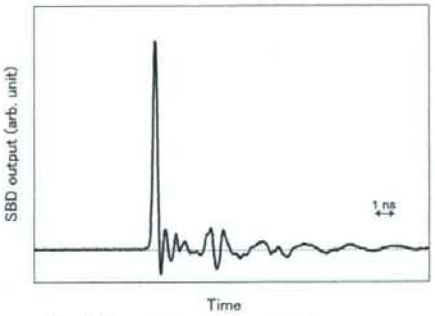

Fig. 9 Temporal waveform of terahertz wave.

用するため，利得曲線に特定周波数における利得の落ち込みが現れる[17]．これは，結晶の損傷しきい値の制約により，計算により予想されていながら観測できなかったスペクトル形である．

Fig. 9に，検出器としてSBDを用いた場合のテラヘルツ光出力の時間波形を示す．受動Qスイッチ動作の励起光源を用いたため，従来の励起光源使用時に比べてQスイッチによる電気雑音の少ない，S/N比の良い信号を観測した．

5. まとめ

小型短パルス，単一縦モード発振，受動Qスイッチ動作のマイクロチップNd:YAGレーザーを励起光源として用いて光源全体の小型化を図ると共に，熱損傷閾値を緩和し，高強度励起による広帯域波長可変，高尖頭値テラヘルツ光源を実現した．15×25 cm^{2}程度の小型テラヘルツ光パラメトリック光源から，波長可変範囲0.9～3.0 THz，発振線幅10 GHz以下，最高出力100 mW(尖頭値)のテラヘルツ光を発生・観測した．この小型励起光源，非線形光学結晶をベースとするコンパクトなテラヘルツ波光源は，常温動作で操作も簡便であり，テラヘルツ領域における応用研究において有力なツールとなることが期待される．

謝　辞

本研究を進めるにあたりご協力いただいた，理研の南出泰亜サブチームリーダー，伊藤弘昌チームリーダー，平山秀樹チームリーダー，緑川克美主任研究員，庄子長一氏，東北大の四方潤一准教授，田久長一氏に深く感謝いたします．また，本研究の一部は，第24回(平成20年度)(財)村田学術振興財団研究助成によって行われました．感謝いたします．

参考文献

1) 斗内政吉：テラヘルツ技術(オーム社，(2006))．
2) P. R. Smith, D. H. Auston, and M. C. Nuss: IEEE J. Quantum Electron. **24** (1998) 255.
3) P. Y. Han and X.-C. Zhang: Appl. Phys. Lett. **73** (1998) 3049.
4) D. M. Mittleman, R. H. Jacobsen, and M. C. Nuss: IEEE J. Sel. Top. Quantum Electron. **2** (1996) 679.
5) R. A. Cheville, R. W. McGowan, and D. Grischkowsky: Phys. Rev. Lett. **80** (1998) 269.
6) J. Allen: Free Electron Lasers and Other Advanced Sources of Light (National Academy Press, Washington, DC. (1994)) 24.
7) S. Komiyama: Phys. Rev. Lett. **48** (1982) 271.
8) E. B. Brown, K. A. McIntosh, K. B. Nichols, and C. L. Dennis: Appl. Phys. Lett. **66** (1995) 285.
9) J. Faist, F. Capasso, D. L. Sivco, C. Sirtori, A. L. Hutchinson, and A. Y. Cho: Science **264** (1994) 553.
10) S. S. Sussman: Microwave Lab. Report No. 1851 (Stanford University (1970)).
11) M. A. Piestrup, R. N. Fleming, and R. H. Pantell: Appl. Phys. Lett. **26** (1975) 418.
12) K. Kawase, J. Shikata, and H. Ito: J. of Phys. D: Appl. Phys. **35** (2002) R1.
13) S. Hayashi, H. Minamide, T. Ikari, Y. Ogawa, J. Shiata, H. Ito, C. Otani, and K. Kawase: Appl. Opt. **46** (2007) 117.
14) Y. R. Shen: *The Principle of Nonlinear Optics* (John Wiley and Sons, New York, (1984)).
15) V. G. Dmitriev, G. G. Gurzadyan, D. N. Nikogosyan eds.: *Handbook of Nonlinear Optical Crystals* (Springer-Verlag, Berlin, (1997)).
16) E. D. Palik ed.: *Handbok of Optical Constants of Solids* (Academic Press, San Diego, (1985)).
17) J. Shikata, K. Kawase, K. Karino, T. Taniuchi, and H. Ito: IEEE Trans. Microwave Theory Tech. **48** (2000) 653.
18) N. Pavel, J. Saikawa, S. Kurimura, and T. Taira: Jpn. J. Appl. Phys. **40** (2001) 1253.
19) H. Sakai, H. Kan, and T. Taira: Opt. Express **16** (2008) 19891.

Terahertz label-free biochip sensor with thin metal mesh

Yuichi Ogawa[1], Shin'ichiro Hayashi[1, 2], Eiji Kato[3], Hisa Yoshida[1], Fumiaki Miyamaru[2], Chiko Otani[2], Kodo Kawase[1, 2, 4]

[1]Tohoku University, [2]RIKEN, [3]Advantest Laboratories Ltd., [4]Nagoya University

Abstract— We demonstrated a biological sensing application using thin metallic mesh — a two-dimensional array of sub-wavelength holes. The band-pass filter property of the thin metal mesh depends not only on its geometrical parameters, but also on the refractive index of the medium in the vicinity of the mesh openings. In order to demonstrate the applicability of this principle in THz biosensing, we used electrospray deposition for realizing a uniform and controllable layer of avidin on a metal mesh substrate. We found out that a quantity of 200 ng/mm^2 electrosprayed avidin produced a distinct shift in the mesh transmission spectrum towards lower frequencies. This observation suggests that it is possible to achieve label-free sensors in the THz range using thin metal mesh sample substrates.

1. Introduction

Many researchers have been investigating various methods for analyzing biomolecules using terahertz (THz) waves [1-6]. This interest is explained by the fact that large molecules exhibiting complex structures have absorption peaks lying in the THz band; for example, the hybridization of DNA and the antigen-antibody reaction can be distinguished without labeling them with fluorescent agents. At present, the THz time-domain spectroscopy (THz-TDS) technique is used for most of the research on biomolecules in the terahertz region. Although THz-TDS is a sensitive detection method, it involves building complex and expensive systems. Consequently, a simpler and cheaper analysis method would be very beneficial.

In parallel, research in the far-infrared using metallic meshes to build band-pass filters has started from around the 1960s. It became clear that the frequency characteristics are determined by geometrical parameters such as the grid's spatial period and aperture size, and application in spectroscopic analysis was suggested [7, 8].

We have been developing a novel sensing method which uses the band-pass characteristics of a thin conductive metal mesh. This sensing method relies on the change in the transmittance of the THz radiation through a metal mesh when a sample substance is inserted in its openings; the transmittance changes not as much because of the absorption in the sample, but mostly because of the different refractive index of the propagation medium near the openings. Our target is to develop a simple and cheap label-free biochip by using a monochromatic light source and a metal mesh.

2. Characteristics of thin metal mesh

Figure 1 shows pattern diagrams of a thin metal mesh (also called an inductive two-dimensional grid) and the equivalent electrical circuit to illustrate its transmission properties. The circuit parameters are determined as functions of the grid geometric parameters [7] and can be calculated approximately from the grating period (g), its thickness (t) and the wire strip width (2a).

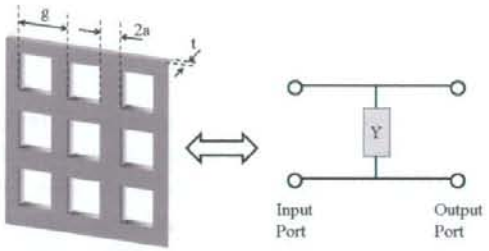

Figure 1. Schematic of the thin metal mesh and the equivalent circuit.

Ulrich's theory shows that at long wavelengths ($g/\lambda < 1$) and for very small thickness ($t \ll \lambda$) the optical properties of the thin metal mesh are conveniently represented as an equivalent electrical circuit by a single admittance (Y) shunting the input. The complex amplitude reflection coefficient of this circuit is

$$\Gamma = -\frac{Y/2}{1+Y/2} \tag{1}$$

In our experiment, the material of metal mesh is electroformed nickel. The thickness of this metal mesh is 5 μm, the grating constant (mesh period) is 63.5 μm, and the side of the square apertures is 45 μm. The transmission spectrum, shown in Figure 2, was measured by FTIR spectroscopy. Figure 2 also shows the calculated transmission spectrum resulting from the geometric parameters of thin metal mesh, based on Ulrich's theory.

This metal mesh behaves as a high-pass filter and the transmittance is approximately 7% at 1 THz. The difference between the experimental curve and the calculated values are relatively small at low frequencies, approximately up to where g/λ is 0.6. Large differences around the peak transmittance are explained by the propagation of diffracted modes [9].

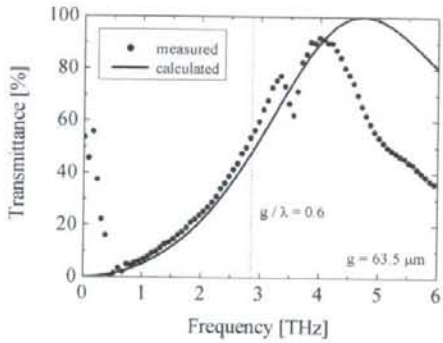

Figure 2. A measured transmission spectrum of the thin metal mesh (•) and its theoretical version calculated using Ulrich's theory (solid line). The dashed line indicates where $g/\lambda = 0.6$.

We first investigated the transmission characteristics of this metal mesh and the way they change depending on the refractive medium in the vicinity of the mesh. For this purpose we coated the mesh with vegetable oil ($n = 1.5$, $k = 0.01$) as a sample. The sample quantity was about 1.0 mg/cm^2 on the mesh. The oil extended uniformly so that its thickness was approximately the same as the metallic mesh, that is, 5 μm.

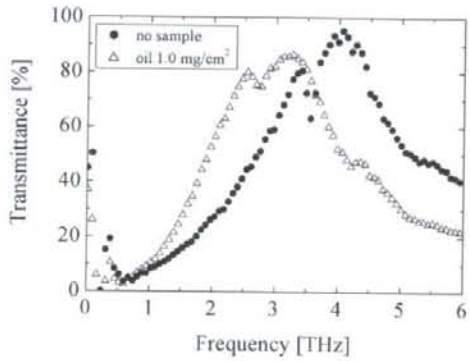

Figure 3. Measured transmission spectra of the thin metal mesh without sample (•) and with vegetable oil as sample (△).

The amplitude of the transmission peak in the spectrum decreases by about 10% when the oil covers the mesh apertures; at the same time the peak frequency drops from 4.1 THz to 3.3 THz. This result demonstrates that the thin metal mesh is sensitive to the refractive index of the sample. Noting that in the frequency range below the peak of the thin metal mesh without sample the transmittance of the thin metal mesh with sample is higher, we conclude that it should also be possible to perform an imaging of the refractive index change at a single frequency.

3. Electrosprayed protein sample

Considering the results presented in the previous section, it is natural to infer that the transmission of the thin metal mesh is also sensitive to biomolecular samples, such as avidin and biotin. The affinity between biotin and avidin is nearly as strong as covalent bonding. To disrupt the complex, extreme denaturing conditions are required. The highly specific and strong binding of the avidin-biotin system has led to its wide usage in a variety of biotechnological applications [4].

In order to apply an avidin sample uniformly and in a controllable quantity, we used the electrospray deposition (ESD) technique [10]. ESD is a versatile method for forming thin films, applicable for solute molecules with a wide range of molecular weights, such as DNA, proteins, and polymers. In the ESD technique, solutions of these materials are transformed into droplet jets; charged electrospray products are deposited onto specific areas of a conductive substrate under control of electrostatic forces. One major advantage of the ESD is that it preserves the functional properties of the electrosprayed biological molecules, such as antigenic and catalytic properties of proteins and hybridization ability of DNA molecules.

In our experiments, electrospraying was carried out using an electrospray deposition device (Esprayer, Fuence Co., Ltd., Japan); the sprayed area was 8 mm in diameter, and the surface density of avidin was 200 ng/mm^2. We investigated the basic sensor property of a thin metal mesh made of nickel (thickness: 6 μm, grid period: 76.2 μm, aperture size: 58 μm). Figure 4 shows the result of transmittance measurements of the thin metal mesh with and without avidin, obtained using an FTIR spectrometer.

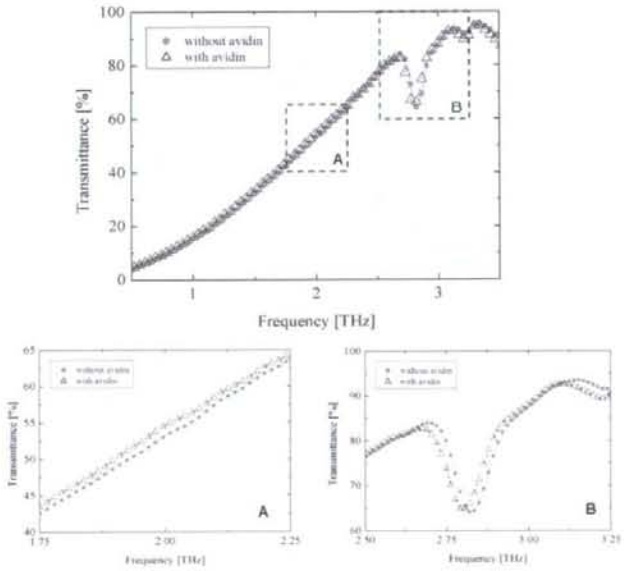

Figure 4. Measured transmission spectra of the thin metal mash without any sample (•) and with avidin (△). Expanded parts of the plot are shown in (A) and (B).

The transmission spectrum of the avidin-sprayed mesh was found to shift towards lower frequencies relative to the bare mesh. As a result, at 2 THz the transmission of the mesh with avidin is approximately 0.8% higher than without avidin. Simultaneously, the resonance absorption peak at 2.82 THz was shifted to 2.79 THz. This shift is believed to be caused by the different refractive index in the vicinity if the metal mesh surface when the small amount of avidin is sprayed on the mesh [11].

4. Conclusion

We demonstrated a sensor application using thin metal mesh, based on the change in the transmission characteristics produced by a variation of the refractive index near the mesh. This result suggests the possibility of realizing a label-free biosensor that may be used, for example, in investigating the biological affinity, such as DNA hybridization and protein interaction. In this report, we will present some detailed results of a sensitivity evaluation of the mesh sensor. Additionally, to confirm the feasibility of biochip sensors, we performed a series of imaging experiments using a monochromatic source at 1 THz.

Acknowledgment

The authors would like to thank Dr. Horoshi Kase and Dr. Kaname Mogami from Fuence Co., Ltd. for allowing us to use their electrospray deposition system.

References

[1] M. Brucherseifer, M. Nagel, P. H. Bolivar, H. Kurz, A. Bosserhoff and R. Büttner: *Appl. Phys. Lett.*, **77**, 4049 (2000)

[2] M. Nagel, P. H. Bolivar, M. Brucherseifer, H. Kurz, A. Bosserhoff and R. Büttner: *Appl. Phys. Lett.*, **80**, 154 (2002).

[3] P. H. Bolivar, M. Brucherseifer, M. Nagel, A. Bosserhoff and R. Büttner: *Phys. Med. and Biol.*, **47**, 3815 (2002).

[4] S. P. Mickan, A. Menikh, H. Liu, C. A. Mannella, R. MacColl, D. Abbott, J. Munch, and X.-C. Zhang, *Phys. Med. Biol.*, **47**, 3789 (2002).

[5] B. Ferguson and X.-C. Zhang, *Nature materials*, **1**, 26 (2002).

[6] A. Menikh, S P. Mickan, H. Liu, R. MacColl, X.-C. Zhang, *Biosensor and Bioelectronics*, **20**, 658 (2004).

[7] R. Ulrich, *Infrared Phys.*, **7**, 37 (1967).

[8] K. Sakai, T. Fukui, Y. Tsunawaki and H. Yoshinaga, *Jpn. J. Appl. Phys.*, **8**, 1046 (2003).

[9] J. M. Laarre, N. Coron, R. Courtin, G. Dambier and M. Charra, *Int. J. Infrared and Millimeter Waves*, **2**, 273 (1981).

[10] V. N. Morozov and T. Ya. Morozova, *Anal. Chem.* **71**, 3110 (1999).

[11] F. Miyamaru, S. Hayashi, C. Otani, K. Kawase, Y. Ogawa, H. Yoshida, E. Kato, *Opt. Lett.*, **31**, 1118 (2006).

THz sensing method based on thin metallic mesh and an application for bimolecular sensing

Eiji Kato[1, 2], Hisa Yoshida[3], Shin'ichiro Hayashi[3, 4], Yuichi Ogawa[3], Kodo Kawase[2, 3, 4]
[1] Advantest Labs. Ltd., 48-2 Matsubara, Kamiayashi, Aoba-ku, Sendai, Japan 989-3124
[2] Nagoya Univ., Furo-cho, Chikusa-ku, Nagoya, Japan 464-8603
[3] Tohoku Univ., 1-1 Amamiya, Tsutsumidori, Aoba-ku, Sendai, Miyagi, Japan 981-8555
[4] RIKEN SENDAI, 519-1399 Aramakiaoba, Aoba-ku, Sendai, Japan 980-0845
eiji.kato@atl.advantest.co.jp

***Abstract*-We report on a novel sensing method in the terahertz (THz) range using thin metallic mesh (TMM). Conventionally, the filter property of a TMM can be changed by the geometrical parameters of the TMM. Considering that it is also change when the medium in the vicinity of the mesh openings has a different refractive index, we inspected this principle. For the biomaterial measurements, we deposited the avidin solution uniformly on the TMM. We observed the change of the transmission characteristics**

I. Introduction

Many researchers have been investigating various methods for analyzing biomolecules using terahertz (THz) waves (see, for example, Ref. [1]). This interest is explained by the fact that large molecules exhibiting complex structures have absorption spectra lying in the THz band. We considered a sensor application using thin metallic mesh (TMM), which is a metallic membrane with a two-dimensional array of sub-wavelength holes. Such TMM is conventionally used as a quasi-optical component. The transmission characteristic of a TMM can be determined by the geometric parameters of the mesh [2]. Since the band-pass properties are also affected when the refractive index of the medium near the mesh openings changes, we can infer that the transmission peak will shift [3]. Consequently, the TMM could work as a simple sensor, sensitive to the refractive index of a sample attached to its surface.

II. Experiments

In order to demonstrate that the TMM has sensitivity to biomolecules, we chose avidin for the sample that has led to its wide usage in a variety of biotechnological applications [4]. To deposit an avidin solution uniformly and in a controllable quantity, we used the electrospray deposition (ESD) technique [5]. In the ESD technique, solution of the sample is transformed into micro droplets with positive charge; the droplets are deposited by electrostatic force onto specific areas of a conductive substrate (TMM). One major advantage of the ESD is that it preserves the functional properties of the electrosprayed biological molecules. In our experiments, we used the ESD equipment (Esprayer, Fuence Co., Ltd. Japan); the sprayed area was 8mm in diameter and the density of avidin was 200 ng/mm^2. We used nickel TMM with grid constant of 76.2 μm for the substrate.

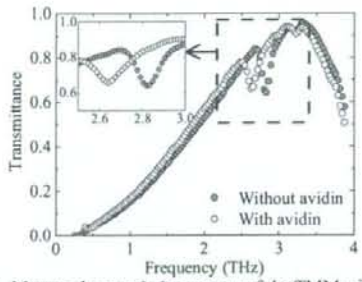

Figure 1. Measured transmission spectra of the TMM without any sample (•) and with avidin (○). The enlarged plot is shown in the inset.

Figure 1 shows the result of transmission measurements of the TMM with and without avidin, obtained using an FTIR spectrometer. The transmission spectrum of the avidin-sprayed mesh was found to shift towards lower frequencies relative to the bare mesh. The dip at 2.82 THz without avidin was shifted to 2.79 THz with avidin. This shift is considered to be caused by the different refractive index in the vicinity if the metal mesh surface when the small amount of avidin is sprayed on the mesh.

III. Conclusion

We demonstrated a sensor application using TMM. This result suggests the possibility of realizing a label-free biosensor that may be used, for example, in investigating the biological affinity.

Acknowledgements

The authors would like to acknowledge for the support Fuence Co., Ltd. for electrospray deposition system.

References

[1] A. Menikh, S P. Mickan, H. Liu, R. MacColl, and X.-C. Zhang, *Biosensor and Bioelectronics*, vol. 20, pp. 658-662, 2004.
[2] K. Sakai, and L. Genzel, *Reviews of Infrared and Millimeter Waves*, vol. 1, Plenum Press, New York, 1983 pp. 155-243
[3] M. Tanaka *et al.*, *Opt. Lett.*, vol. 30, pp. 1210-1212, 2005
[4] S. P. Mickan *et al.*, *Phys. Med. Biol.*, vol. 47, pp. 3789-3795, 2002
[5] V. N. Morozov and T. Y. Morozova, *Anal. Chem.*, vol. 71, pp. 3110-3117, 1999.

Compact Terahertz-Wave Parametric Generators

S. Hayashi[1, 3], H. Minamide[2], T. Ikari[2], Y. Ogawa[3], T. Shibuya[1], K. Shindo[1], H. Sakai[4], H. Kan[4], T. Taira[5], H. Ito[2, 6], C. Otani[1], and K. Kawase[1, 3, 7]

[1]RIKEN, 2-1 Hirosawa, Wako, Saitama, 351-0198, Japan,
[2]RIKEN Sendai, 519-1399 Aramaki-Aoba, Aoba-ku, Sendai, 980-0845 Japan,
[3]Graduate School of Agricultural Science, Tohoku Univ., 1-1 Tsutsumidori Amamiyamachi, Aoba-ku, Sendai 981-8555, Japan
[4]Central Research Lab., Hamamatsu Photonics K. K., 5000 Hirakuchi, Hamamatsu 434-8601, Japan
[5]Laser Research Center for Molecular Science, Institute for Molecular Science, Myodaiji, Okazaki 444-8585, Japan
[6]RIEC, Tohoku Univ., 2-1-1 Katahira, Aoba-ku, Sendai 980-8577, JAPAN
[7]Dept. of Quantum Eng., Nagoya Univ., Furo-cho, Chikusa-ku, Nagoya 464-8601, Japan
Author e-mail address: shayashi@riken.jp

Abstract: We developed two new kinds of terahertz-wave parametric generators (TPG) by using compact pump sources. One TPG generates high energy and broadband THz-waves with high stability, the other has a potential to be a narrow-linewidth injection-seeded TPG.

1. Introduction

In recent years, Terahertz (THz) wave sources have received considerable attention for use in many applications. Especially, recent researches using THz-waves, transparency and fingerprint spectra have had an important contribution in the Bioengineering or Security fields. As you know, the subject of research decides the source specifications. For example, to study the environment or living plants, experiments must be performed outside the laboratory. Then, you need high energy, portable sources and detectors. In spectroscopic studies, you need widely tunable sources. Analyzing or detecting gasses requires a narrow linewidth. Consequently, the goal is to have customized sources for each application. In this paper, we introduce two compact THz-wave parametric sources with different characteristics. One generates high energy, broadband and stabilized THz-wave, the other has a potential of widely tunability and narrow linewidth. The characteristics of there sources depend on its pump source. The former is for transmitting detection of samples with high absorption coefficient or diffuse detection. The later is for on site spectroscopic measurement of samples.

2. Principle of the THz-wave Parametric Generation

In a TPG, generation of the THz-waves is achieved through an efficient parametric scattering of laser light via a polariton - stimulated polariton scattering. The scattering process involves both second- and third-order nonlinear processes. Thus, strong interaction occurs among the pump, the idler, and the polariton (THz) waves.

The principle of THz-wave generation is as follows. Polaritons exhibit phonon-like behaviour in the resonant frequency region. However, they behave like photons in the off-resonant low-frequency region, where a signal photon at THz frequency (ω_T) and a near-infrared idler photon (ω_i) are parametrically created from a near-infrared pump photon (ω_p), according to the energy conservation law $\omega_p = \omega_T + \omega_i$ (p: pump; T: THz; i: idler). In the stimulated scattering process, the momentum conservation law $\boldsymbol{k}_p = \boldsymbol{k}_i + \boldsymbol{k}_T$ (noncolinear phase-matching condition; see the inset in Fig. 1) also holds. This leads to angle-dispersive characteristics of the idler- and THz-waves. The bandwidth of the TPG depends on the parametric gain and the absorption coefficients in the THz region. More details about TPG are given in Refs. [1].

3. Experimental setup

The experimental apparatus, shown in Fig. 1, consists of a pump source and two nonlinear crystals. About energy enhancement version, we used compact Q-sw. Nd:YAG laser as a pump source. All components, except for the detector, can be mounted on a 12 × 22 cm breadboard. The pump beam is collimated by a lens at the output of the source and reflected by mirrors for downsizing of a source. It has a top-hat profile with a beam diameter of 1.3 mm (FWHM) on the first crystal. We used two 65-mm-long nonlinear $MgO:LiNbO_3$ crystals. A Si-prism array placed on the y surface of the second crystal acts as an efficient output coupler for the THz-waves to avoid the total internal reflection of the THz-waves on the crystal output side. For an efficient THz-wave emission, the pumped region within the second crystal must be as close as possible to the Si-prism array, because of the large

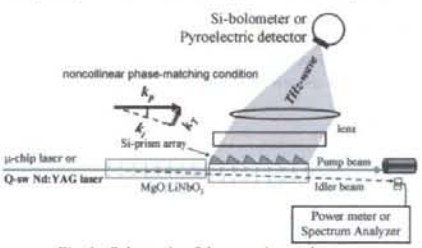

Fig. 1: Schematic of the experimental setup.

absorption coefficient of the $MgO:LiNbO_3$ crystal in the 1 ~ 3 THz range (10 ~ 100 cm^{-1}). A top-hat beam profile is suitable for this purpose, since the high intensity region of the pump beam is closer to the *y* surface than in the case of a Gaussian beam. The distance between the *y* surface and the beam center was precisely adjusted to obtain a maximum THz-wave output, and it was approximately equal to the pump beam radius. The THz-wave output extracted through the Si-prism array was measured using a 4.2 K Si bolometer, while the idler-wave energy was measured using a pyroelectric detector.

About another source for narrow linewidth, we replace pump source to microchip laser [2]. All components except for the detector can be mounted within an area of 25 × 5 cm^2. This pump source is a diode end-pumped single-mode microchip Nd^{3+}:YAG laser passively Q-sw. by Cr^{4+}:YAG saturable absorber. This microchip configuration enables the low order axial and transverse mode laser oscillation, which linewidth is below 0.009 nm. The laser delivers 1.8 MW peak power pulses (750 μJ/pulse) with 420 ps pulse width at 100 Hz repetition rate with a M^2 factor of 1.09. This laser is free from the electric noise compared with active Q-sw. lasers. Additionally, this kind fixed passively Q-switching allows us the stabilized peak power, less than +/- 2% power jitter [2]. The pump beam diameter on the first crystal is 0.3 mm (FWMH). We used a pyroelectric sensor to detect both the THz-wave and the idler-wave.

4. Experimental results

First, we show experimental results of high energy TPG. The output energy of the THz-wave reached 105 pJ/pulse (62 mW at the peak) when the pump energy is 66 mJ/pulse (820 MW/cm^2) [3]. In our previous TPG research, the damage threshold of the crystal was under 200 MW/cm^2 of pump beam when using multimode pump source. With this report, the damage threshold is increased about 4 times. We generated 100 times more output energy by higher energy pumping and lower absorption due to the short pulsed, top-hat distribution of the pump beam. Fig. 2 shows the stability of the THz-wave pumped by this pump source. We measured the pulse-to-pulse energy stability and found that it is 3.8 %rms. This value shows that its stability is about ten times better than other THz-wave parametric sources.

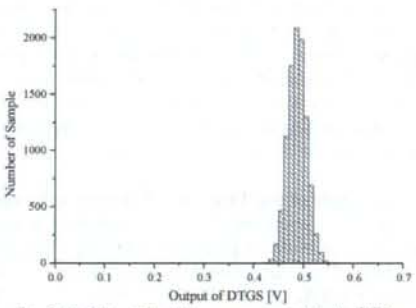

Fig. 2: Stability of the THz-wave generated by the TPG.

Second, we show some results about narrow linewidth TPG. The characteristics of the generated THz-wave is depends on that of pump beam. To generate narrow linewidth THz-wave, narrow linewidth pump beam is required. We replaced above pump source to microchip laser. As the pump energy is increased above the generation threshold, the energy of the idler wave increases linearly. The maximum energy of the idler wave is 110 μJ/pulse, obtained at a pump energy of 750 μJ/pulse (2.9 GW/cm^2). When using the previous singlemode pump laser with 15 ns pulse width, the damage threshold of the crystal was 450 MW/cm^2, but in this experiment the crystal is not damaged even when pumped by 2.9 GW/cm^2 [4]. The short pulse width of the microchip laser allows the pumping power to be about 5 times higher. We observed an output energy of the THz-wave of about 0.1 pJ/pulse (1 mW at the peak) when the pump intensity is 2.9 GW/cm^2 [3].

5. Conclusion

We demonstrated two new kinds of palmtop TPG by using compact pump sources. We showed the output power enhancement, high stability and the downsizing of the TPG pumped by multimode Nd:YAG laser with tophat beam profile. We expect its broadband, high energy, stability and palm-top size offer good advantages for many applications. We also observed THz-wave output pumped by single-mode microchip Nd:YAG laser. This TPG has a potential of narrow linewidth THz-wave by injection seeding for the idler wave.

Acknowledgements

The authors would like to acknowledge the continuing encouragement of Prof. J. Nishizawa. The authors thank C. Takyu for his excellent work coating the crystal surface, and T. Shoji for polishing the crystals superbly.

References

[1] J. Shikata, K. Kawase, T. Taniuchi, and H. Ito, *Jpn. J. Appl. Phys.*, **41**, 134 (2002)
[2] N. Pavel, J. Saikawa, S. Kurimura, and T. Taira, *Jpn. J. Appl. Phys.*, **40**, pt. 1, no. 3A, 1253 (2001).
[3] S. Hayashi, K. Maki, C. Otani, and K. Kawase, Proceedings of the International symposium TOPICAL PROBLEMS OF NONLINEAR PHYSICS, High-field Laser Physics (NWP-2), pp 50-51 (2005).
[4] K. Kawase, J. Shikata, and H. Ito, *J. Phys. D: Appl. Phys.*, **34**, R1 (2001).

Microlaser Pumped Narrow-linewidth Terahertz-Wave Parametric Generation

S. Hayashi[1, 2], T. Shibuya[1, 3], H. Sakai[4], H. Kan[4], T. Taira[5], Y. Ogawa[2], C. Otani[1], and K. Kawase[1, 2, 3]
[1]RIKEN SENDAI, 519-1399 Aramakiaoba, Aoba, Sendai, 980-0845 JAPAN
[2]Graduate School of Agricultural Science, Tohoku Univ., 1-1 Tsutsumidori Amamiyamachi, Aoba, Sendai, 981-8555 JAPAN
[3]Graduate School of Engineering, Nagoya Univ. Furo-cho, Chikusa, Nagoya, 464-8603 JAPAN
[4]Hamamatsu Photonics K. K., 5000 Hiraguti, Hamamatsu, 434-8601 JAPAN
[5]Institute for Molecular Science, 38 Nishigo-Naka, Myodaiji, Okazaki, 444-8585 JAPAN
shayashi@riken.jp

Abstract- **We developed injection-seeded terahertz wave parametric generator pumped by microlaser. Microlaser is the half palm-sized, LD-pumped single-mode microchip Nd:YAG laser, delivers 1.1 MW peak power pulses (530 μJ/pulse) with 430 ps pulse width at 100 Hz repetition rate. This THz-wave source generated narrow-linewidth THz-wave by injection seeding for the idler-wave. We observed its peak output power of more than 20 mW (2 pJ/pulse) at 1.6 THz and its palm size, portable source offer good advantages for many applications.**

I. Introduction

In recent years, Terahertz (THz) wave sources have received considerable attention for use in many applications. Especially, recent researches using THz-waves, transparency and fingerprint spectra have had an important contribution in the bioengineering or security fields. As you know, the subject of research decides the source specifications. For example, to study the environment or living plants, experiments must be performed outside the laboratory. Then, you need high energy, portable sources and detectors. In spectroscopic studies, you need widely tunable sources. Analyzing or detecting gasses requires a narrow linewidth. Consequently, the goal is to have customized sources for each application. In this paper, we introduce compact, tunable and narrow linewidth THz-wave parametric source.

II. Principle of the THz-wave Parametric Generation

In a THz-wave parametric generation, generation of the THz-waves is achieved through an efficient parametric scattering of laser light via a polariton - stimulated polariton scattering. The scattering process involves both second- and third-order nonlinear processes. Thus, strong interaction occurs among the pump, the idler, and the polariton (THz) waves. Polaritons exhibit phonon-like behavior in the resonant frequency region. However, they behave like photons in the off-resonant low-frequency region, where a signal photon at THz frequency ($\omega_{THz\text{-}wave}$) and a near-infrared idler photon (ω_{idler}) are parametrically created from a near-infrared pump photon (ω_{pump}), according to the energy conservation law $\omega_p = \omega_{THz} + \omega_i$. In the stimulated scattering process, the momentum conservation law $\boldsymbol{k}_p = \boldsymbol{k}_i + \boldsymbol{k}_T$ (noncolinear phase-matching condition) also holds. This leads to angle-dispersive characteristics of the idler- and THz-waves. More details about TPG are given in Refs. [1].

III. Experimental Setup

The experimental setup consists of a pump source, seeding source and nonlinear crystal. This pump source is a diode end-pumped single-mode microchip Nd^{3+}:YAG laser passively Q-sw. by Cr^{4+}:YAG saturable absorber. This microchip configuration enables the low order axial and transverse mode laser oscillation, which linewidth is below 0.009 nm. The laser delivers 1.1 MW peak power pulses (530 μJ/pulse) with 430 ps pulse width at 100 Hz repetition rate with a M^2 factor of 1.09. This laser is free from the electric noise compared with active Q-sw. lasers. Additionally, this kind fixed passively Q-switching allows us the stabilized peak power, less than +/- 2 % power jitter [2]. The pump beam diameter on the first crystal is 0.3 mm (FWMH). We used a 4K Si-bolometer to the THz-wave.

IV. Experimental Results

Figure 1 shows time dependent THz-wave output signals measured by the 4K Si-bolometer. When we generate THz-wave without injection seeding to the idler-wave, we observed broadband THz-wave with power of about 1 mW at the peak (lower curve), however, after injection seeding, we observed narrow linewidth THz-wave with power of about 20 mW at the peak (upper curve). This is about more than 100 times narrower and 20 times higher than seeding laser is cut off. In addition, the pulse width of this microlaser is the shortest in our parametric sources [3, 4].

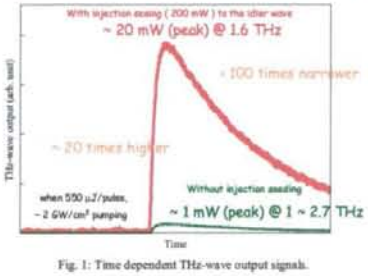

Fig. 1: Time dependent THz-wave output signals.

V. Conclusion

We demonstrated compact, tunable and narrow linewidth THz-wave source. We observed THz-wave output pumped by single-mode microchip Nd:YAG laser. This source generates narrow linewidth THz-wave by injection seeding for the idler wave. We expect this source offer good advantages for many applications.

Acknowledgements

The authors thank Dr. Minamide, Dr. Ikari, Dr. Shikata, and Prof. Ito for useful discussion, Mr. C. Takyu for his excellent work coating the crystal surface, and Mr. T. Shoji for polishing the crystals superbly. This work was supported in part by a Grant-in-Aid for Young Scientist (No. 17760290) from Ministry of Education, Culture, Sports, Science and Technology.

References

[1] J. Shikata, K. Kawase, T. Taniuchi, and H. Ito, *Jpn. J. Appl. Phys.*, **41**, 134 (2002).
[2] N. Pavel, J. Saikawa, S. Kurimura, and T. Taira, *Jpn. J. Appl. Phys.*, **40**, pt. 1, no. 3A, 1253 (2001).
[3] S. Hayashi, K. Maki, C. Otani, and K. Kawase, *Proc. SPIE*, **5975**, 219 (2006).
[4] K. Kawase, J. Shikata, and H. Ito, *J. Phys. D: Appl. Phys.*, **34**, R1 (2001).

THz sensing method based on metallic mesh and application to high-resolution sensing and imaging

E. Kato, S. Yoshida, H. Yoshida, A. Hayashi, S. Hayashi, Y. Ogawa, C. Otani and K. Kawase

Abstract— **We report on a sensing method in the terahertz range using metallic mesh (MM). Conventionally, the filter property of an MM can be changed by the geometrical parameters of the MM. Considering that this property is also changed when the medium in the vicinity of the mesh openings has a different permittivity, we were able to measure small amounts of absorbing materials and thin plastic films on the metallic mesh. We observed change of both the transmission characteristics and the images.**

Index Terms—**imaging, metallic mesh, sensing, surface wave**

I. Introduction

Metallic meshes (MMs), metallic membranes with a two-dimensional array of sub-wavelength holes, have been used as quasi-optical components such as mirrors, beam splitters, filters, and Fabry-Perot interference filters in the spectral region from microwave to far infrared [1]. The transmission characteristics of MMs can be determined by the shape and the arrangement of the apertures [2], [3]. The phenomenon of resonance enhanced transmission peaks observed for MMs is attributed not only to the waveguide mode but also to the resonant excitation of surface waves at the metal-air (or dielectric) boundaries of MMs [4]. Since the resonant frequency and transmittance are strongly affected by changes in the dielectric constant of the medium near the mesh openings, we can infer that small amounts of samples, attached on the metal surface, can be detected with high sensitivity [5].

E. Kato is with the Advantest Labs. Ltd., Sendai 989-3124 Japan (e-mail: eiji.kato@jp.advantest.com).

H. Yoshida and Y. Ogawa are with the Graduate School of Agricultural Science, Tohoku University, Sendai 981-8555, Japan (email: yoshida_h@bios.tohoku.ac.jp; yogawa@bios.tohoku.ac.jp).

A. Hayashi, S. Hayashi and C. Otani are with Terahertz-wave Research Program, RIKEN, Sendai 980-0845, Japan (email: ahayashi@riken.jp; shayashi@riken.jp; otani@riken.jp).

S. Yoshida and K. Kawase are with the EcoTopia Science Institute, Nagoya University, Nagoya 464-8603, Japan (email: h076433m@mbox.nagoya-u.ac.jp; kawase@nuee.nagoya-u.ac.jp).

II. Experiments

A. Transmission properties of MM

We measured the basic transmission property of bare MM. Fig. 1 shows the transmission spectrum of the bare MM produced by the electroforming method with a focused beam under normal incidence using a standard THz-TDS system. The schematic of the MM is shown in the inset of Fig. 1. The grid constant of the MM is $g = 254$ μm, wire strip width $2a = 74$ μm and thickness $t = 60$ μm. The enhanced transmission peak is observed at frequencies around 1 THz. The maximum transmittance at 1.03 THz is two times higher than that expected from the porosity of the mesh holes, and there exists one sharp dip at 0.99 THz. This sharp dip is attributed to anomalous diffraction when the THz wave incidents to the MM obliquely, similar to Wood's anomaly [6].

B. THz sensing of small amount of samples using MM

To investigate the quantitative responsiveness of the MM as a sensor, we used a commercial ink-jet printer (Pixus BJ F900, Canon, Tokyo, Japan) for quantitative ink sample ($n \sim 2.1$, $\kappa \sim 0.2$) spread. The amount of ink sample was controlled using image processing software. We prepared two types of substrates for comparison: the MM and a 0.1 mm thick PET film. The printed ink density on the PET film substrates was 40, 45 and 50 ng/mm^2, respectively. Given that the porosity of the MM holes is about 50%, the estimated density of the ink printed on the MM is one-half that of the PET film substrate. For this

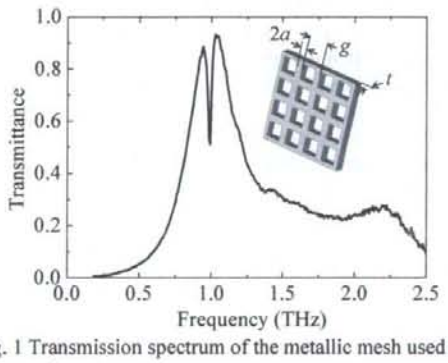

Fig. 1 Transmission spectrum of the metallic mesh used in the experiment.

1-4244-1439-3/07/$25.00 ©2007 IEEE

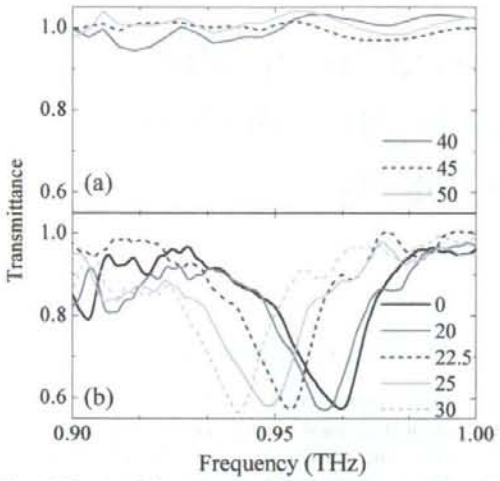

Fig. 2 Transmission spectra of printed ink samples. (a) without MM, (b) with MM. Unit of ink density is ng/mm^2.

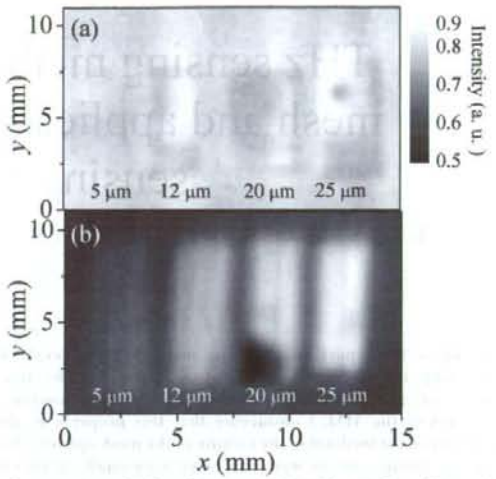

Fig. 3 Transmission image of the thin Teflon films. (a) without MM. (b) with MM.

experiment, we set up a spectroscopic and imaging system using a backward wave oscillator (BWO) as a THz wave source (0.85 ~ 1.10 THz) and a deuterated L-alanine triglycine sulphate (DLATGS) detector [7]. THz waves radiating from the BWO are collimated by an off-axis parabolic mirror and focused onto the sample by another mirror. For image acquisition, the sample is x-y scanned using a linear motor stage that moves it through the focused beam. Fig. 2(a) shows the transmission spectra of the PET film substrate with the aforementioned densities of ink. There is no significant change even at higher ink densities. Fig. 2(b) shows the transmission spectra of the MM substrates with some ink densities and without ink. The lower shift of dip frequencies with increasing ink density is clearly observed relative to the bare MM, and a difference of 2.5 ng/mm^2 ink density could be detected; such a difference is difficult to detect using conventional THz spectroscopy. These shifts are believed to be caused by changes in the dielectric constant in the vicinity of the MM surface when small amounts of ink are printed on the MM.

C. *THz imaging of thin materials using MM*

For highly sensitive sensing by imaging, we used thin free-standing Teflon foils (Nilaco Co., Tokyo, Japan) of 5, 12, 20 and 25 μm thickness as samples. We attached the samples on both 0.1 mm thick paper and the MM, and imaged them using the aforementioned experimental setup. Fig. 3(b) of the THz transmission image of the samples attached on the MM at 0.96 THz shows that the thickness of the samples could be determined based on the transmitted power, and a difference of 5 μm thickness could be distinguished. However, such a difference could not be determined for the paper since there is no detectable contrast even for increased sample thickness (Fig. 3(a)).

III. Conclusion

We demonstrated highly sensitive sensing using MM, based on changes in the transmission characteristics produced by a variation of the dielectric constant near the mesh openings. Small amounts of absorbing substances printed on the MM can thus be detected, and a film sample much thinner than the THz wave can also be distinguished by imaging. This result suggests the possibility of label-free sensing of biological affinities, such as in the case of DNA hybridization or protein interactions, and a method for producing a simple, inexpensive sensor chip using a printing technology. We plan to investigate the MM sensor mechanism in further detail and will attempt to enhance its present sensitivity.

References

[1] K. Sakai, T. Fukui, Y. Tsunawaki and H. Yoshinaga, "Metallic mesh bandpass filters and Fabry-Perot interferometer for the far infrared," *Jpn. J. Appl. Phys.*, vol. 8, no. 8, pp.1046-1055, Aug. 1969

[2] R. Ulrich, "Far-infrared properties of metallic mesh and its complementary structure," *Infrared Phys.*, vol. 7, iss. 1, pp.37-55, Jan. 1967.

[3] K. Sakai and L. Genzel, "Far-infrared metal mesh filter and Fabry-Perot interferometry," in *Reviews of Infrared and Millimeter Waves*, vol. 1, K. J. Button, Ed. New York: Plenum, 1983, pp. 155-247

[4] H. F. Ghaemi, T. Thio, D. E. Grupp, T. W. Ebbesen and H. J. Lezec, "Surface plasmons enhance optical transmission through subwavelength holes," *Phys. Rev. B*, vol. 58, iss. 11, pp. 6779-6782, Sep. 1998.

[5] F. Miyamaru, S. Hayashi, C. Otani, K. Kawase, Y. Ogawa, H.Yoshida and E. Kato, "Terahertz surface-wave resonant sensor with a metal hole array," *Opt. Lett.*, vol. 31, iss. 8, pp. 1118-1120, Apr. 2006.

[6] J. M. Lamarre, N. Coron, R. Courtin, G. Dambier and M. Charra, "METALLIC MESH PROPERTIES AND DESIGN OF SUBMILLIMETER FILTERS," *Int. J. Infrared Millimeter Waves*, vol. 2, no. 2, pp. 273-292 Mar. 1981.

[7] A. Dobroiu, C. Otani and K. Kawase, "Terahertz-wave sources and imaging applications," *Meas. Sci. Technol.*, vol. 17, no. 11, pp.R161-R174, Nov. 2006.

Label-free Immunoassay by the Resonant Transmission Phenomenon of a Thin Metallic Mesh

Hisa Yoshida[1], Yasuhide Kawai[1], Shin'ichiro Hayashi[2], Eiji Kato[3], Masato Oikawa[4], Teruo Miyazawa[1], Chiko Otani[5], Kodo Kawase[6] and Yuichi Ogawa[1]

1. Graduate School of Agricultural Science, Tohoku University, Sendai, Japan
2. Laser Technology Laboratory, RIKEN, Wako, Japan
3. ADVANTEST Laboratories, Ltd. Sendai, Japan
4. Graduate School of Life Sciences, Tohoku University, Sendai, Japan
5. Terahertz-wave Research Program, RIKEN, Sendai, Japan
6. EcoTopia Science Institute, Nagoya University, Nagoya, Japan

Abstract:
We propose a new label-free sensor of protein using a metallic mesh in Terahertz (THz) region. Our sensing method relies on a change in the transmittance of THz radiation passed through the metallic mesh on which a sample substance is contacted. Label-free detection using THz radiation is a new technique in biomedicine, which enable us to take easier and faster medical and food inspections.

By using this technique, we demonstrated the highly sensitive detection the protein horseradish peroxidase, which is an oxidation/reduction enzyme that exists in many organisms. For quantitative investigation of the sensitivity of our sensor, the enzyme was printed on surface of the metallic mesh by a commercial printer. A distinct shift in the transmittance spectrum toward lower frequency was observed for 500 pg/mm^2 (11 fmol) enzyme printed on the metallic mesh. Next we demonstrated to detect a streptavidin-biotin interaction on a PVDF membrane which is generally used fixation of protein and DNA. The streptavidin-biotin interaction can be detected by using 650 pg/mm^2 (2.5 pmol) biotin. These results indicate that our sensing system has high sensitivity and we have successfully demonstrated a convenient sensing system by using a metallic mesh and a PVDF membrane.

Keywords: *label-free immunoassay, metallic mesh, Terahertz radiation, membrane*

1. INTRODUCTION

Immunoassay is one of the most popular methods in biomedicine, which is based on antigen/antibody reaction using specific antibody. This method generally needs label materials, which might involve fluorescence, an enzyme reaction, or radioisotope, for highly sensitive detection. However the procedure is complex and takes a lot of time. On the other hand, Terahertz (THz) technology has broad applicability in a biomedical context and facilitates various applications because the collective vibration modes of many protein and DNA molecules are predicted to occur in the THz range.

In this paper, we propose a label-free sensing method using a thin metallic mesh in the THz region. The transmission characteristics of thin metallic meshes, investigated since the 1960s [1,2], are those of a band-pass filter in the far-infrared region. This is due to the resonant transmission caused by an excitation of surface plasmon polaritons (SPPs) [3]. The transmission properties of a thin metallic mesh are determined mainly by its geometric parameters, but, when a material is placed near the mesh openings, are also affected by the refractive index of that material, in the sense that a shift of the resonant transmission frequency occurs. [4,5] Our sensing method is based on the change of the transmittance of THz radiation through a thin metallic mesh accompanied by the resonant frequency shift when a sample substance is applied on the mesh openings. The transmittance of the thin metallic mesh does not change due to the absorption, but dominantly due to the variation of the refractive index of the sample substances near the openings [6]. Using this thin metallic mesh sensor, we detected the protein horseradish peroxidase, which is an oxidation/reduction enzyme existing in many organisms and is typically used as an indicator in biochemical reactions. Horseradish peroxidase is one of the most widespread label substrates in biomedicine. Next by using PVDF membrane and a thin metallic mesh, we have demonstrated to detect streptavidin (240 kDa)-biotin complex.

2. EXPERIMENT

2.1 Properties of a thin metallic mesh

In our experiment, the thin metallic mesh was made from electroformed nickel, allowing the fabrication of a smooth surface and precise periodicity of the grating. The two dimensional square metallic mesh was 6 μm thick with a grating period of 76.3 μm and a metallic line width of 18.3 μm, in both dimensions. This metallic mesh behaves as a high-pass filter and the peak transmission is approximately 95 % at 2.8 THz. We measured the transmission spectra of a thin metallic mesh using a Fourier Transform Infrared (FT-IR) spectrometer (FARIS-1S; JASCO, Japan), in which the THz beam was focused into an area of about 5 mm in diameter on the thin metallic mesh.

Figure 1 shows the transmission spectrum of thin metallic mesh as a function of the wavelength λ normalized by the grating period g. The transmittance at the peak

Corresponding author: H. Yoshida, yoshida_h@bios.tohoku.ac.jp

wavelength observed at $\lambda / g = 1.23$, which is slightly longer than $\lambda / g = 1$, is 1.65 times as high as the opening fraction of the metallic mesh (57.8 %). This resonant transmission phenomenon is based on the interference effect between the THz waves transmitted directly through metal openings and reemitted from the surface plasmon polaritons excited on the metal surface [7,8]. In addition, a sharp transmission dip is observed at wavelength of $\lambda / g = 1.5$. This transmission dip appears as the result of the splitting of the surface plasmon polariton modes for the oblique incidence [9] derived by the focused THz radiation beam in our experimental setup. Since the resonant frequencies of the transmission peak and dip strongly depend on the refractive index in the vicinity of the metallic mesh openings, the extremely small amount of the sample substances can be detected by monitoring the position of the transmission peak and/or dip.

2.2 Highly sensitive detection of a protein horseradish peroxidase

We used the protein horseradish peroxidase (Nacalai Tesque) as a sample, by dissolving it in sterilized pure water at the concentrations of 1.0, 0.5, 0.25, and 0.125 mg/ml. These enzyme solutions were spread on the thin metallic mesh. For a quantitative investigation of the sensitivity of the metallic mesh sensor, the accurate spreading of sample substances on the sensor is critically important. We printed horseradish peroxidase on the metallic meshes using a commercial inkjet printer (Pixus 860i; Canon, Tokyo, Japan), the same that was previously used to fix DNA on a chip [10]. The amount of the sample was controlled using an image processing software. By using the inkjet printer, a considerably small amount of sample can be spread on various materials more readily than with other printing systems.

Figure 2(a) shows the measured transmission spectra of the thin metallic mesh with various amounts of peroxidase printed on it. We present the transmission spectra only in the wavelength range around the transmission dip observed in Fig. 2. The transmission dip frequency shows a tendency to decrease with increasing the amount of sprayed peroxidase. The transmission dip frequency, which is estimated from the fitting of the measured spectrum with a Lorentz function, is plotted in Fig. 2(b) as a function of the amount of peroxidase. A clear frequency shift of the transmission dip is observed for 500 – 2100 pg/mm^2 horseradish peroxidase with respect to that of the bare metallic mesh (0 pg/mm^2). This result indicates that the sensing with thin metallic meshes is extremely sensitive for the detection of very small amounts of biomolecules, equal to the sensitivity of the conventional method using an antibody labeled horseradish peroxidase. The peak frequency basically shifts to the lower frequency side with increasing the volume of the horseradish peroxidase in the range from 300 to 2100 pg/mm^2. The peak frequency for 2100 pg/mm^2, however, returns slightly to the higher frequency with respect to that for 1100 pg/mm^2. This result is due to the inhomogeneous spreading of the horseradish peroxides on the metallic mesh in our printing system. More precise spreading can help to avoid this ambiguity in the detection of the frequency shift.

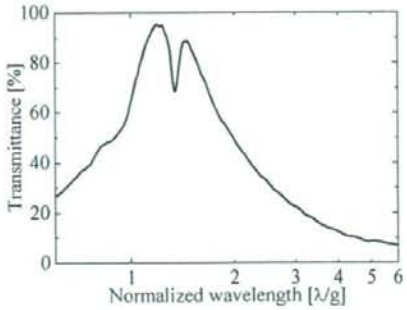

Fig.1. Measured transmission spectrum of a thin metallic mesh with grating period of 76.3 μm and a metallic line width of 18.3 μm.

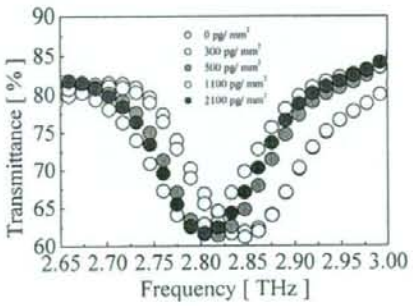

(a)

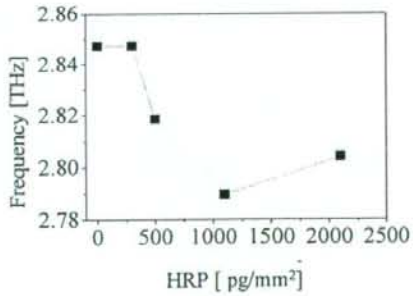

(b)

Fig. 2. (a) Measured transmission spectra of a thin metallic mesh with various concentrations of horseradish peroxidase. (b) The transmission dip frequency as a function of the horseradish peroxidase.

The transmittance at the dip frequency changes only slightly with the volume of the horseradish peroxides. This indicates that the absorption of the THz wave by the sample substances plays a minor role for the variation of the transmission spectrum. Such a small variation of the transmittance makes it difficult to detect the sample sub-

stances by monitoring the transmission intensity at a single frequency. However, owing to the shift of the resonant frequency depending on the refractive index in the vicinity of the metallic openings, a sensitive detection of the sample substances becomes possible with the single frequency source in the THz regime. In our experiments, a variation of more than 18 % in the transmission is observed at 2.9 THz for 1100 pg/mm^2 with respect to the bare metallic mesh. If we assume that the uncertainty of the transmittance in our experimental setup is less than 1 %, it follow s that we can detect the horseradish peroxides of at least 60 pg/mm^2 (a few fmol), which is never detected by conventional THz spectroscopy.

2.3 Detection of streptavidin-biotin interaction on PVDF membrane

Streptavidin (240 kDa) is a protein which binds biotin. Streptavidin-biotin complex has a low dissociation constant of about 10^{-15} M. Bovine serum albumin (BSA) (Alubumin bovine serum, powder ;SIGMA) was labeled biotin (EZ-Link Sulfo-NHS-Biotinylation Kit: Pierce Biotechnology, Inc.) and applied on PVDF membrane(Immun-Blot™ PVDF Membrane; Bio-Rad) which generally used for fixation protein and DNA. These membrane which put in biotinylated-BSA, were into 0.1 % BSA solution (0.1 % BSA 20mM Tris, 500 mM NaCl, 0.05 % Tween-20, pH 7.5) for a prevention that other protein were attached these membrane. Stereptavidin-biotin interaction was occurred in TTBS buffer (20 mM Tris, 500 mM NaCl, 0.05 % Tween-20, pH 7.5), after the process these membrane were washed TTBS buffer and pure water.

A thin metallic mesh (6 μm thick with a grating period of 76.3 μm and a metallic line width of 18.3 μm,) was fixed a circular holder and adhered with these membrane using a suction pump. We measured the transmission spectra of a thin metallic mesh with membrane using a Fourier Transform Infrared (FT-IR) spectrometer.

The transmission dip frequency, which is estimated from the fitting of the measured spectrum with a Lorentz function, is plotted in Fig. 3 as streptavidin-biotin interaction. When PVDF membrane was set on the metallic mesh, the peak frequency shiftt to the lower frequency side. This phenomenon based on a refractive index of PVDF membrane. In a case of biotinylated-BSA were applied on PVDF membrane, the peak frequency further

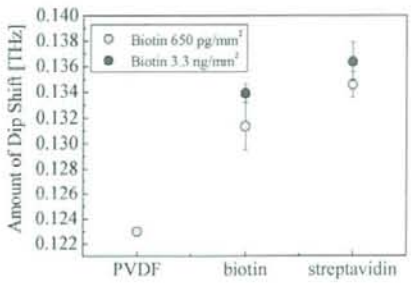

Fig. 3. The transmission dip frequency as streptavidin-biotin interaction.

shift to the lower frequency side. Finally streptavidin bind to biotinylated-BSA, amount of a dip shift was largest in the reaction. The refractive index of streptavidin-biotin complex was larger than biotinylated-BSA. Amount of dip shift increased on a concentration of biotin. The measurement of a transmittance without the metallic mesh could not detect streptavidin-biotin interaction. In our label-free sensing using the metallic mesh, 650 pg/mm^2 (2.5 pmol) biotin could be detected by the shift.

3. CONCLUSION

In conclusion, we demonstrated the highly sensitive detection of protein molecules in amounts in the fmol order by using a thin metallic mesh sensor. For spreading the extremely small amount of sample substances on the metallic mesh sensor, we used a commercially available printer. For the metallic mesh sensor printed with 500 pg/mm^2 (11 fmol) horseradish peroxidase, a red-shift of the the transmission dip frequency is observed clearly, which is based on the variation of the refractive index in the vicinity of the metallic mesh openings. This result exceeds the detection limit of conventional THz spectroscopy for protein molecules. Next we have successfully demonstrated a label-free detection of streptavidin-biotin interaction on a PVDF membrane. The streptavidin-biotin interaction can be detected by using 650 pg/mm^2 (2.5 pmol) biotin. These results indicates that our sensing system has high sensitivity and we have successfully demonstrated a convenient system by using a metallic mesh and PVDF membrane. As a next challenge, we aim to achieve a label-free selective detection of proteins by using an antigen/antibody reaction.

ACKNOWLEDGEMENTS

This work was supported in part by a Grant-in-Aid for Young Scientists (18070501) from The Ministry of Health, Labour and Welfare of Japan.

REFERENCES

1. R. Ulrich, *Infrared Physics*, **7**, 37 (1967).
2. K. Sakai, T. Fukui, Y. Tsunawaki, and H. Yoshinaga, *Jpn. J. Appl. Phys.*, **8**, 1046 (1969).
3. H. Raether, *Surface Plasmons on Smooth and Rough Surfaces and on Gratings* (Springer-Verlag, Berlin, 1988).
4. F. Miyamaru and M. Hangyo, *Appl. Phys. Lett.*, **84**, 2742 (2004).
5. H. Cao and A. Nahata, *Opt. Exp.*, **12**, 1004 (2004).
6. F. Miyamaru, S. Hayashi, C. Otani, K. Kawase, Y. Ogawa, H. Yoshida, and E. Kato, *Opt. Lett.*, **31**, 1118 (2006).
7. L. Martin-Moreno, F. J. Garcia-Vidal, H. J. Lezec, K. M. Pellerin, T. Thio, J. B. Pendry, and T. W. Ebbesen, *Phys. Rev. Lett.*, **86**, 1114 (2001).
8. E. Popov, M. Neviere, S. Enoch and R. Reinisch, *Phys. Rev. B*, **62**, 16100 (2000).
9. H. F. Ghaemi, T. Thio, D. E. Grupp, T. W. Ebbesen, and H. J. Lezec, *Phys. Rev. B.*, **58**, 6779 (1998).
10. T. Okamoto, T. Suzuki and N. Yamamoto, *Nature Biotech.*, **18**, 438 (2000).

Tunable Terahertz-wave Parametric Generation pumped by Microchip Nd:YAG laser

S. Hayashi[1,2], T. Shibuya[1,3], H. Sakai[4], H. Kan[4], T. Taira[5], Y. Ogawa[2], C. Otani[1], and K. Kawase[1,2,3]

[1]RIKEN SENDAI, 519-1399 Aramakiaoba, Aoba, Sendai, 980-0845 JAPAN
[2]Tohoku Univ., 1-1 Tsutsumidori Amamiyamachi, Aoba, Sendai, 981-8555 JAPAN
[3]Nagoya Univ. Furo-cho, Chikusa, Nagoya, 464-8603 JAPAN
[4]Hamamatsu Photonics K. K., 5000 Hiraguti, Hamamatsu, 434-8601 JAPAN
[5]Institute for Molecular Science, 38 Nishigo-Naka, Myodaiji, Okazaki, 444-8585 JAPAN

Abstract: We have developed THz-wave parametric generator pumped by microchip Nd:YAG laser. This generated tunable, narrow-linewidth THz-wave with injection seeding by external cavity diode laser (ECDL) for the idler-wave. We observed THz-wave tunable range from 1.6 to 3.0 THz, linewidth of less than 10 GHz.

OCIS codes: (140.3070) Infrared and far-infrared lasers; (190.2620) Frequency conversion; (190.4360) Nonlinear optics, devices; (190.4410) Nonlinear optics, parametric processes; (190.4970) Parametric oscillators and amplifiers

I. Introduction

In recent years, the technologies available in the terahertz (THz) frequency range, connecting the microwaves and the infrared, have made great progress with the development of new methods for generating and detecting the THz radiation. Especially, recent researches using THz-waves, transparency imaging and fingerprint spectra have had an important contribution in the bioengineering or security fields. One of the most prominent applications of the THz technologies is in the spectroscopy for characterizing various materials, such as medicine[1], saccharides[2], and so on. The achievements of the THz spectroscopy made the application range widen even further, allowing, for example, the nondestructive inspection of mail envelopes for illegal drugs[3] and the quality evaluation of agricultural products[4]. With the existence of numerous characteristic vibration modes of macro-molecules such as proteins[5] or the DNA[6] confirmed in the THz region, the sensing of proteins[7], the label-free probing of the DNA[8], and the label-free bioaffinity detection[9] have attracted great attention. In this paper, we developed our tunable injection seeded THz-wave parametric generator[10,11] pumped by microchip Nd:YAG laser for spectroscopic study. This source generates tunable and narrow linewidth THz-wave by injection seeded for the idler beam by ECDL.

II. Principle of the THz-wave Parametric Generation

When a strong laser beam propagates through a nonlinear crystal, photon and phonon transverse wave fields are coupled, behave as new mixed photon-phonon states, called polaritons. The generation of the THz wave results from the efficient parametric scattering of laser light via a polariton, that is, stimulated polariton scattering. The scattering process involves both second- and third-order nonlinear processes. Thus, strong interaction occurs among the pump beam, the idler wave, and the polariton (THz) wave. The principle of tunable THz wave generation is as follows. The polaritons exhibit phonon-like behavior in the resonant frequency region (near the TO-phonon frequency ω_{TO}). However, they behave like photons in the non resonant low-frequency region as shown in Fig. 1, where a signal photon at THz frequency (ω_T) and a near-infrared idler photon (ω_i) are created parametrically from a near-infrared pump photon (ω_p), according to the energy conservation law $\omega_p = \omega_T + \omega_i$ (p: pump beam, T: THz wave, i: idler wave). In the

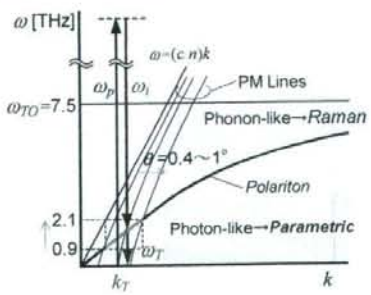

Figure 1: Dispersion relation of the polariton.

stimulated scattering process, the momentum conservation law $k_p = k_i + k_T$ (noncollinear phase-matching condition, Fig. 2) also holds. This leads to the angle-dispersive characteristics of the idler and THz waves. Thus, broadband THz waves are generated depending on the phase-matching angle. Generation of a coherent THz wave can be achieved by applying an optical resonator (in the case of the TPO) or injecting a "seed" for the idler wave (in the case of the is-TPG). Continuous and wide tunability is accomplished simply by changing the angle between the incident pump beam and the resonator axis or the seed beam.

The bandwidth of the TPG is decided by the parametric gain and absorption coefficients in the THz region. Figure 3 shows the calculated gain and the absorption coefficient at several pump intensities. The gain curve has a broad bandwidth of around 3 THz, with a dip appearing at around 2.6 THz. This is because the low frequency modes of doped MgO in the $MgO:LiNbO_3$ work as a crystal lattice defects for $LiNbO_3$.

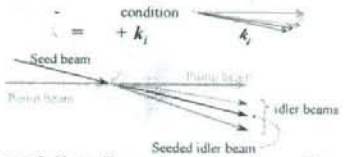

Figure 2: Noncollinear phase matching condition.

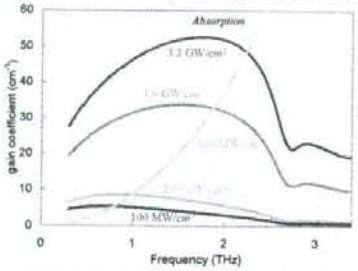

Figure 3: The calculated gain coefficient.

III. Experimental setup

The experimental setup, shown in Fig. 4, consists of a pump source (Microchip Nd:YAG laser), seeding source (ECDL) and nonlinear crystal. This pump source is a diode end-pumped single-mode microchip Nd^{3+}:YAG laser passively Q-sw. by Cr^{4+}:YAG saturable absorber. This microchip configuration enables the low order axial and transverse mode laser oscillation, which linewidth is below 0.009 nm. The laser delivers 1.1 MW peak power pulses (530 μJ/pulse) with 430 ps pulse width at 100 Hz repetition rate with a M^2 factor of 1.09. This laser is free from the electric noise compared with active Q-sw. lasers. Additionally, this kind fixed passively Q-switching allows us the stabilized peak power, less than +/- 2 % power jitter[12]. The pump beam diameter on the first crystal is 0.3 mm (FWMH). We used two 65-mm-long nonlinear $MgO:LiNbO_3$ crystals. A Si-prism array placed on the y surface of the second crystal acts as an efficient output coupler for the THz-waves to avoid the total internal reflection of the THz-waves on the crystal output side. For an efficient THz-wave emission, the pumped region within the second crystal must be as close as possible to the Si-prism array, because of the large absorption coefficient of the $MgO:LiNbO_3$ crystal in the 1 ~ 3 THz range (10 ~ 100 cm^{-1}). The distance between the y surface and the beam center was precisely adjusted to obtain a maximum THz-wave output, and it was approximately equal to the pump beam radius. The THz-wave output extracted through the Si-prism array was measured using a 4.2 K Si-bolometer, while the idler-wave energy was measured using a pyroelectric detector.

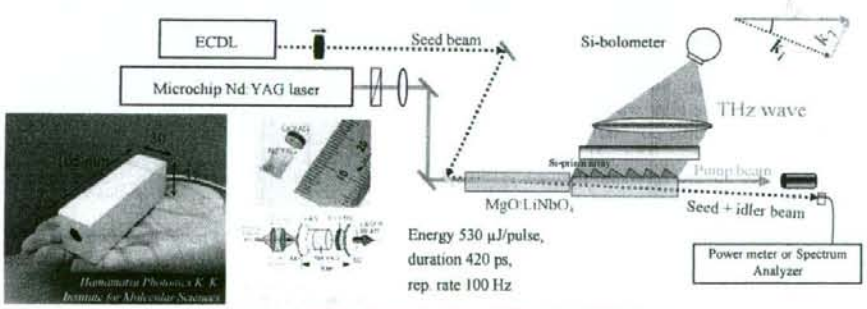

Figure 4: Experimental setup and picture of Microchip Nd:YAG laser.

IV. Experimental Results

Figure 5(a) shows tunability of our THz-wave source by a scanning Fabry–Perot etalon consisting of two Ni metal mesh plates with 65 μm grid. The displacement of one of the metal mesh plates corresponds directly to half of the wavelength. When the pump energy was 530 μJ/pulse (power of 1.1 MW (peak), intensity of 2.0 GW/cm^2) and seeding power of 100 mW, we observed the THz-wave wavelength from 113 – 144 μm (frequency of 2.04 – 2.65 THz) by changing wavelength of the idler wave and the angle between the pump beam and the idler wave satisfying phase matching condition. Figure 5(b) shows an example of wavelength and linewidth measurement. We observed narrow linewidth THz-wave with wavelength of 147 μm and power of about 20 mW at the peak by the 4K Si-bolometer. The free spectral range (FSR) of the etalon was about 100 GHz, and the linewidth was measured to be less than 10 GHz.

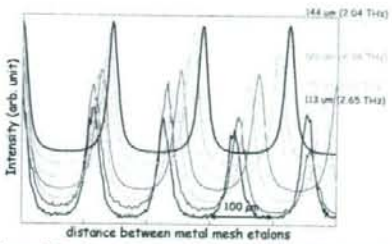

Figure 5(a): Tunability by scanning Fabry – Perot etalon.

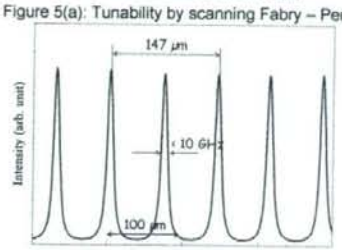

Figure 5(b): An example of wavelength and linewidth measurement.

V. Conclusion

We demonstrated compact and tunable THz-wave source pumped by microchip Nd:YAG laser. This source generates narrow linewidth (< 10 GHz) and tunable (113 – 144 μm (frequency of 2.04 – 2.65 THz)) THz-wave by injection seeding for the idler wave. We expect this source offers good advantages for many spectroscopic applications.

Acknowledgements

The authors thank Dr. Minamide, Dr. Ikari, Dr. Shikata, Prof. Ito, Dr. Hirayama, and Dr. Midorikawa for useful discussion, Mr. C. Takyu for his excellent work coating the crystal surface, and Mr. T. Shoji for polishing the crystals superbly. This work was supported in part by a Grant-in-Aid for Young Scientist (No. 17760290) from Ministry of Education, Culture, Sports, Science and Technology.

References

[1] Y. Watanabe, K. Kawase, and T. Ikari, *Appl. Phys. Lett.*, **83**, 800 (2003).
[2] M. Hineno and H. Yoshinaga, Spectrochimica Acta, **30A**, 411 (1974).
[3] K. Kawase, Y. Ogawa, and Y. Watanabe, *Opt. Exp.*, **11**, 2549 (2003).
[4] Y. Ogawa, S. Hayashi, N. Kondo, K. Ninomiya, C. Otani and K. Kawase, ASABE (The American Society of Agricultural and Biological Engineers) 2006 Annual International Meeting Technical Papers, Paper Number : 063050 (2006).
[5] B. Brooks and M. Karplus, *Proc. Natl. Acad. Sci.*, **80**, 6571 (1983).
[6] L. L. Van Zandt and V. K. Saxena, *Phys. Rev. A*, **39**, 2672 (1989).
[7] A. Markelz, S. Whitmire, J. Hillebrecht, and R. Brige, *Phys. Med. Biol.* **47**, 3797 (2002).
[8] M. Brucherseifer, M. Nagel, P. Haring Bolivar, and H. Kurz, *Appl. Phys. Lett.*, **77**, 4049 (2000).
[9] S. P. Mickan, A. Menikh, H. Liu, C. A Mannella, R. MacColl, D. Abbott, J. Munch, and X.-C. Zhang, *Phys. Mes. Biol.*, **47**, 3789 (2002).
[10] S. Hayashi, K. Maki, C. Otani, and K. Kawase, *Proc. SPIE*, **5975**, 219 (2006).
[11] K. Kawase, J. Shikata, and H. Ito, *J. Phys. D: Appl. Phys.*, **34**, R1 (2001).
[12] N. Pavel, J. Saikawa, S. Kurimura, and T. Taira, *Jpn. J. Appl. Phys.*, **40**, pt. 1, no. 3A, 1253 (2001).

Injection-seeded THz wave Parametric Generator using Microchip Nd:YAG Laser

Shin'ichiro Hayashi

RIKEN, 519-1399 Aramakiaoba, Aoba, Sendai, 980-0845 JAPAN
Graduate School of Agricultural Science, Tohoku University, 1-1 Tsutsumidori Amamiyamachi, Aoba, Sendai, 981-8555 JAPAN

shayashi@riken.jp

Abstract: We have realized tunable terahertz wave parametric generator by using microchip Nd:YAG laser and observed output terahertz wave with tuning range of 0.9 – 3 THz, peak power of about 100 mW, and detected by schottky barrier diode.

1. Introduction

In recent years, Terahertz (THz) wave sources have received considerable attention for use in many applications. Especially, recent researches using THz waves, transparency imaging and fingerprint spectra have had an important contribution in the bioengineering or security fields. As you know, the specifications of source are decided by targets. For example, to study the environment or living plants, experiments must be performed outside the laboratory. Then, you need portable sources and detectors. In spectroscopic studies, you need widely tunable sources. Analyzing or detecting gasses requires a narrow linewidth. In this paper, we introduce compact and tunable THz wave parametric source pumped by microchip Nd:YAG laser, seeded for the idler wave by extended cavity diode laser (ECDL) and detected by schottky barrier diode (SBD).

2. Principle of the THz wave Parametric Generation

When a strong laser beam propagates through a nonlinear crystal, photon and phonon transverse wave fields are coupled, behave as new mixed photon-phonon states, called polaritons. The generation of the THz wave results from the efficient parametric scattering of laser light via a polariton, that is, stimulated polariton scattering. The scattering process involves both second- and third-order nonlinear processes. Thus, strong interaction occurs among the pump beam, the idler wave, and the polariton (THz) wave. The principle of tunable THz wave generation is as follows. The polaritons exhibit phonon-like behavior in the resonant frequency region (near the TO-phonon frequency ω_{TO}). However, they behave like photons in the non resonant low frequency region as shown in figure 1, where a signal photon at THz frequency (ω_T) and a near-infrared idler photon (ω_i) are created parametrically from a near-infrared pump photon (ω_p), according to the energy conservation law $\omega_p = \omega_T + \omega_i$ (p: pump beam, T: THz wave, i: idler wave). In the stimulated scattering process, the momentum conservation law $\boldsymbol{k_p = k_i + k_T}$ (noncollinear phase-matching condition, figure 1) also holds. This leads to the angle-dispersive characteristics of the idler and THz waves. Thus, broadband THz waves are generated depending on the phase-matching angle. Generation of a coherent THz wave can be achieved by applying an optical resonator (in the case of the TPO) or injecting a "seed" for the idler wave (in the case of the is-TPG). Continuous and wide tunability is accomplished by changing the wavelength of seed beam and the angle between the incident pump beam and the resonator axis[1]. The bandwidth of the TPG is decided by the parametric gain and absorption coefficients in the THz region[2].

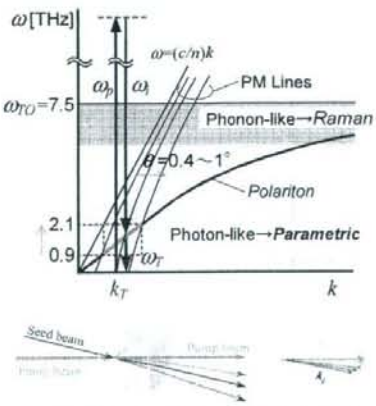

Figure 1: Dispersion relation of the polariton and noncollinear phase matching condition.

3. Experimental setup

The experimental setup, shown in figure 2, consists of a pump source (Microchip Nd:YAG laser), seeding source (ECDL) and nonlinear crystal ($MgO:LiNbO_3$). This pump source is a diode end-pumped, single-mode microchip Nd^{3+}:YAG laser passively Q-switched by Cr^{4+}:YAG saturable absorber. This microchip configuration enables the

978-1-4244-1932-6/08/$25.00 ©2008 IEEE

low order axial and transverse mode laser oscillation, which linewidth is below 0.009 nm. The laser delivers 1.3 MW peak power pulses (650 μJ/pulse) with 520 ps pulse width at 100 Hz repetition rate with a M^2 factor of 1.09. This laser is free from the electric noise compared with active Q-switched lasers. Additionally, this kind fixed passively Q-switching allows us the stabilized peak power, less than +/- 2 % power jitter[3]. The pump beam diameter on the first crystal is 0.3 mm (FWMH). We used two 65-mm-long nonlinear MgO:$LiNbO_3$ crystals. A Si-prism array placed on the y surface of the second crystal acts as an efficient output coupler for the THz waves to avoid the total internal reflection of the THz waves on the crystal output side. For an efficient THz wave emission, the pumped region within the second crystal must be as close as possible to the Si-prism array, because of the large absorption coefficient of the MgO:$LiNbO_3$ crystal in the 1 – 3 THz range (10 – 100 cm^{-1}). The distance between the y surface and the beam center was precisely adjusted to obtain a maximum THz-wave output, and it was approximately equal to the pump beam radius. The THz-wave output extracted through the Si-prism array was measured using a 4.2 K Si-bolometer or schottky diode (SBD), while the idler wave was measured using a optical spectrum analyzer.

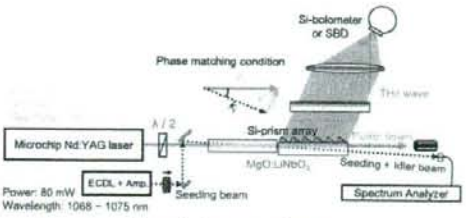

Figure 2: Experimental setup.

4. Experimental results

It was possible to tune the THz wavelength using an ECDL as a tunable seeder. When the pump intensity was 1.8 GW/cm^2 (peak, energy of 650 μJ/pulse) and seeding power of 80 mW (CW), a wide tunability from 0.95 – 2.9 THz was observed as shown in figure 3 by changing both the seed wavelength and the seed incident angle. The maximum output power of THz wave was about 100 mW (peak) at around 1.8 THz. The tuning curve has a broad bandwidth, with a dip appearing at around 2.6 THz. This is because the low frequency modes of doped MgO in the MgO:$LiNbO_3$ work as crystal lattice defects for $LiNbO_3$[4].

Figure 4 shows time dependent signal detected by SBD. It is advantageous to detect THz wave from our source because output signal from SBD depends on peak power and microchip laser is free from electrical noise. In our experimental condition, signal-to-noise (S/N) ratio is more than 100. Compared with our previous pump source with conventional Q-switched Nd:YAG laser, the S/N ratio dramatically improved.

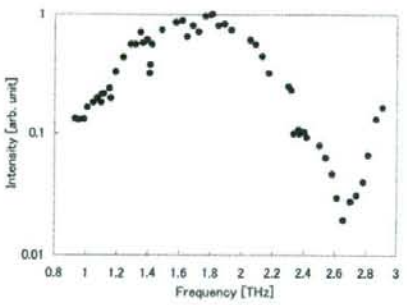

Figure 3: Wide tunability of is-TPG.

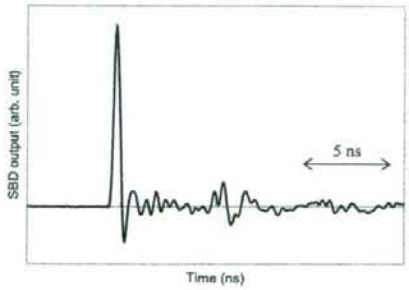

Figure 4: An example of time dependent signal detected by SBD.

5. conclusion

We demonstrated compact and tunable THz wave source pumped by microchip Nd:YAG laser. This source generates tunable THz wave by injection seeding for the idler wave with high peak power. We could also observe generated THz wave by SBD. In this case, this source and detector worked at room temperature. We expect this source offer good advantages for many applications.

References

[1] K. Kawase, J. Shikata, and H. Ito, *J. Phys. D: Appl. Phys.*, **34**, R1 (2001).
[2] J. Shikata, K. Kawase, T. Taniuchi, and H. Ito, *Jpn. J. Appl. Phys.*, **41**, 134 (2002).
[3] N. Pavel, J. Saikawa, S. Kurimura, and T. Taira, *Jpn. J. Appl. Phys.*, **40**, pt. 1, no. 3A, 1253 (2001).
[4] J. Shikata, K. Kawase, K. Karino, T. Taniuchi, and H. Ito, *IEEE Trans. Microwave Theory Tech.*, **48**, 653 (2000).